

Supplementary Information

M. Feygenson,^{1,2,3}, Z. Huang⁴, Y. Xiao⁴, X. Teng⁵, W. Lohstroh⁶, N. Nandakumaran⁷, J. C. Neuefeind⁸, M. Everett⁸, A. A. Podlesnyak⁸, G. Salazar-Alvarez³, S. Ulusoy³, M. Valvo⁹, Y. Su¹⁰, S. Ehlert², A. Qdemat⁷, M. Ganeva¹⁰, L. Zhang¹¹, M. C. Aronson¹²

¹*European Spallation Source ERIC, SE-221 00 Lund, Sweden*

²*Jülich Centre for Neutron Science (JCNS-1) at*

Forschungszentrum Jülich, D-52425 Jülich, Germany

³*Department of Materials Science and Engineering,*

Uppsala University, Box 35, 751 03, Uppsala, Sweden.

⁴*School of Advanced Materials, Peking University,*

Shenzhen Graduate School, Shenzhen 518055, China

⁵*Worcester Polytechnic Institute, Department*

of Chemical Engineering, Worcester 01609, USA

⁶*Heinz Maier-Leibnitz Zentrum (MLZ), Technische Universität München,*

Lichtenbergstr. 1, 8574 Garching, Germany

⁷*Jülich Centre for Neutron Science (JCNS-2) and Peter Grünberg Institute (PGI-4),*

Jülich GmbH, 52425, Jülich, Germany

⁸*Neutron Scattering Division, Oak Ridge National Laboratory,*

Oak Ridge, Tennessee 37831, USA

⁹*Department of Chemistry, Uppsala University, 75121 Uppsala, Sweden*

¹⁰*Jülich Centre for Neutron Science (JCNS-4) at Heinz Maier-Leibnitz-Zentrum (MLZ),*

Forschungszentrum Jülich GmbH, Lichtenbergstr. 1, 85747 Garching, Germany

¹¹*Center for Functional Nanomaterials, Brookhaven National Laboratory,*

Upton, New York 11973-5000, USA and

¹²*Stewart Blusson Quantum Matter Institute,*

University of British Columbia, Vancouver, BC V6T 1Z4, Canada

I. X-RAY POWDER DIFFRACTION DATA

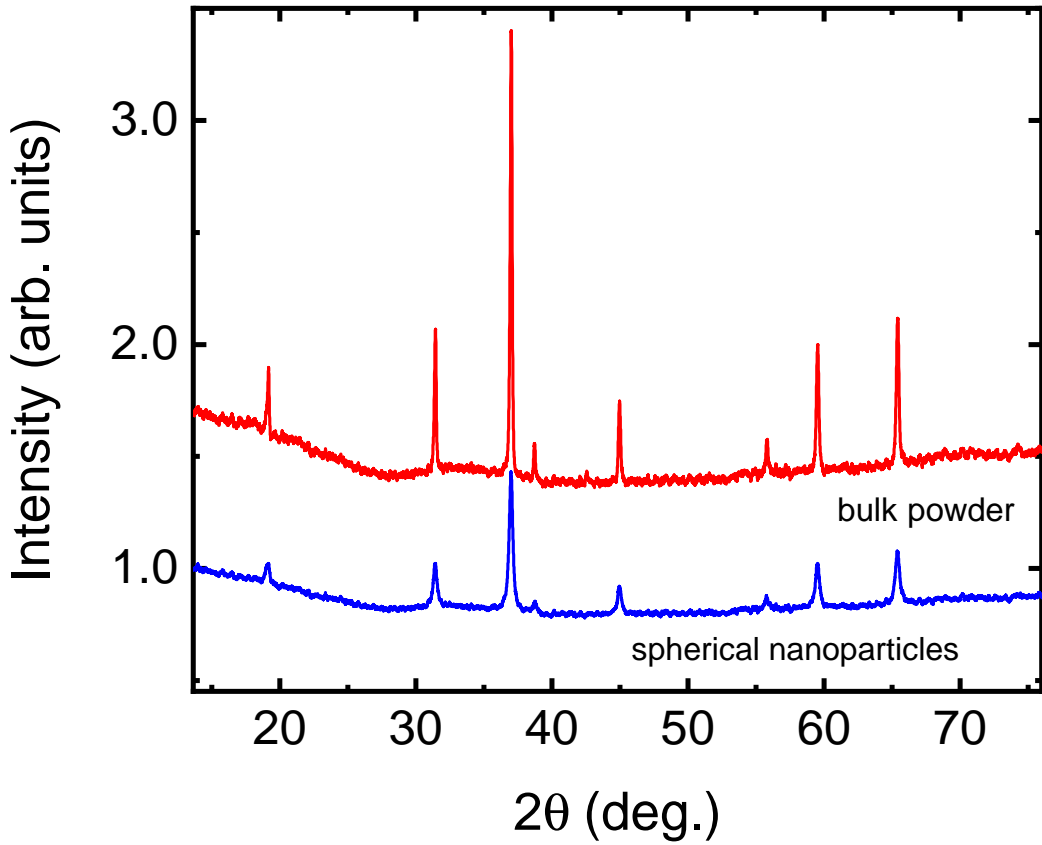


FIG. S1. Room temperature x-ray powder diffraction measurements with the wavelength of 1.54 Å of the bulk powder and spherical nanoparticles. The bulk powder data is offset for clarity.

II. RAMAN SCATTERING MEASUREMENTS

The most intense Raman mode around 692 cm^{-1} (A_{1g}) is typically ascribed to characteristic symmetric stretching motions of the oxygen in the octahedral units [1–4], although some ambiguity exists in the assignation of this peak and different scenarios have been suggested [5]. A hypothesis that the A_{1g} mode could involve both symmetric M_{tet} –O stretching of the oxygen in the tetrahedral site and deformation of the M_{oct} –O bond in the three octahedral sites nearest to each oxygen [6] was also put forward and this would depend on the Co^{2+} and

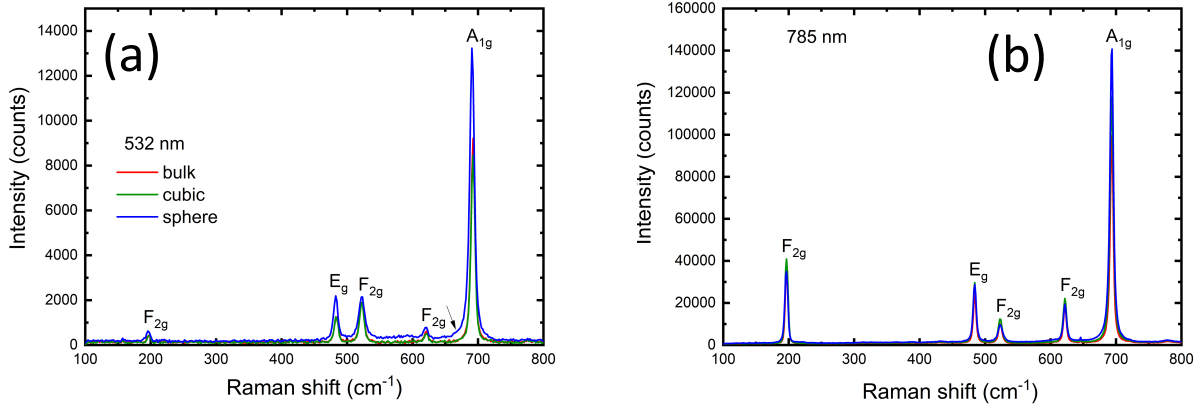


FIG. S2. Comparison of as-recorded Raman spectra for the three samples obtained via excitation wavelengths of (a) 532 nm and (b) 785 nm. Note that the spherical nanoparticles yield in both cases the highest Raman scattering intensity for the strongest A_{1g} symmetric vibration. A slight red-shift of the A_{1g} and F_{2g} modes, respectively located at high and low wavenumbers, is seen in (a) together with a clear broadening of all the peaks only for the spherical nanoparticles, while no peak shift and broadening is otherwise observed in (b).

TABLE S1. Positions and approximate FWHM of the various Raman peaks obtained upon excitation via a 532 nm laser wavelength. The peak position and FWHM were obtained from the fit of the peaks with a Gaussian function. All units are in cm^{-1} .

Sample	F_{2g}		E_g		F_{2g}		F_{2g}		A_{1g}	
	Position	FWHM	Position	FWHM	Position	FWHM	Position	FWHM	Position	FWHM
bulk	197.3(5)	4.0(1.0)	483.6(2)	6.4(3)	522.6(1)	7.5(2)	620.8(4)	5.7(7)	692.4(1)	6.5(1)
cubic	197.5(4)	4.4(8)	483.4(2)	6.3(3)	522.5(1)	7.1(2)	620.9(4)	5.9(8)	692.4(1)	6.5(1)
sphere	196.2(7)	5.2(1.4)	482.6(2)	7.5(4)	522.5(3)	11.2(5)	619.6(9)	12.5(1.9)	690.9(1)	8.2(1)

Co^{3+} occupations. The E_g and F_{2g} modes in the 450-650 cm^{-1} range are possibly related to combined vibrations of the tetrahedral site and octahedral oxygen motions [1, 3, 7, 8]. The F_{2g} mode around 200 cm^{-1} is typically related to the movement of the tetrahedral sites and was ascribed to a complete translation of the tetrahedral unit within the spinel lattice [2, 5].

TABLE S2. Positions and approximate FWHM of the various Raman peaks obtained upon excitation via a 785 nm laser wavelength. The peak position and FWHM were obtained from the fit of the peaks with a Gaussian function. All units are in cm^{-1} .

Sample	F_{2g}		E_g		F_{2g}		F_{2g}		A_{1g}	
	Position	FWHM								
bulk	196.8(1)	4.5(1)	484.2(1)	4.7(2)	523.2(2)	5.9(4)	621.9(1)	4.9(2)	693.5(1)	5.4(1)
cubic	196.7(1)	4.6(1)	484.1(1)	5.3(2)	523.2(2)	6.3(4)	621.9(1)	5.8(2)	693.5(1)	6.1(1)
sphere	196.4(1)	4.7(2)	484.2(1)	5.2(2)	523.3(4)	7.9(8)	621.9(1)	5.6(3)	693.4(1)	6.2(1)

III. RIETVELD AND PDF REFINEMENTS RESULTS

TABLE S3. Summary of the Rietveld and PDF refinements of averaged and local ($r=1.5\text{-}10 \text{ \AA}$) crystal structures at 10 K.

Rietveld				PDF		
sample	Spher.	Cubic	Bulk	Spher.	Cubic	Bulk
a,b,c (\AA)	8.0753(1)	8.0865(5)	8.0863(3)	8.0744 (8)	8.0800(9)	8.0791(8)
m (μ_B)	2.756(5)	2.883(4)	3.00(4)			
R_p	4.30%	4.97%	5.30%			
GOF	4.98	2.68	2.94			
R_{wp}				15.2%	12.8%	11.5%

TABLE S4. The Rietveld and PDF refinements ($r=1.6\text{-}20$ Å) results for all samples at 10 K.

Rietveld

Spherical						Cubic					
Atom	x	y	z	Occ.	U_{iso} (Å 2)	x	y	z	Occ.	U_{iso} (Å 2)	
Co1	0	0	0	0.92(2)	0.0076(4)	0	0	0	1.0	0.0040(6)	
Co2	0.6250	0.6250	0.6250	0.93(2)	0.0076(5)	0.6250	0.6250	0.2500	1.0	0.0040(6)	
O	0.3881	0.3881	0.3881	0.92(2)	0.0076(5)	0.3881	0.3881	0.3881	1.0	0.0039(4)	

Bulk					
Atom	x	y	z	Occ.	U_{iso} (Å 2)
Co1	0	0	0	1.0	0.0018(5)
Co2	0.6250	0.6250	0.6250	1.0	0.0018(5)
O	0.3881	0.3881	0.3881	1.0	0.0018(5)

PDF

Spherical						Cubic					
Atom	x	y	z	Occ.	$U_{11,22,33}$ (Å 2)	x	y	z	Occ.	$U_{11,22,33}$ (Å 2)	
Co1	0.1250	0.1250	0.1250	0.87(3)	0.0020(7)	0.1250	0.1250	0.1250	0.97(4)	0.0034	
Co2	0.5000	0.5000	0.5000	0.98(2)	0.0016(4)	0.5000	0.5000	0.5000	0.94(5)	0.0041(4)	
O	0.2635	0.2635	0.2635	1.0(4)	0.0042(2)	0.2635	0.2635	0.2635	1.0(5)	0.0048(6)	

Bulk					
Atom	x	y	z	Occ.	$U_{11,22,33}$ (Å 2)
Co1	0.1250	0.1250	0.1250	1.0	0.0027(4)
Co2	0.5000	0.5000	0.5000	1.0	0.0015(3)
O	0.2635	0.2635	0.2635	1.0	0.0039(2)

IV. DIFFUSE NEUTRON SCATTERING

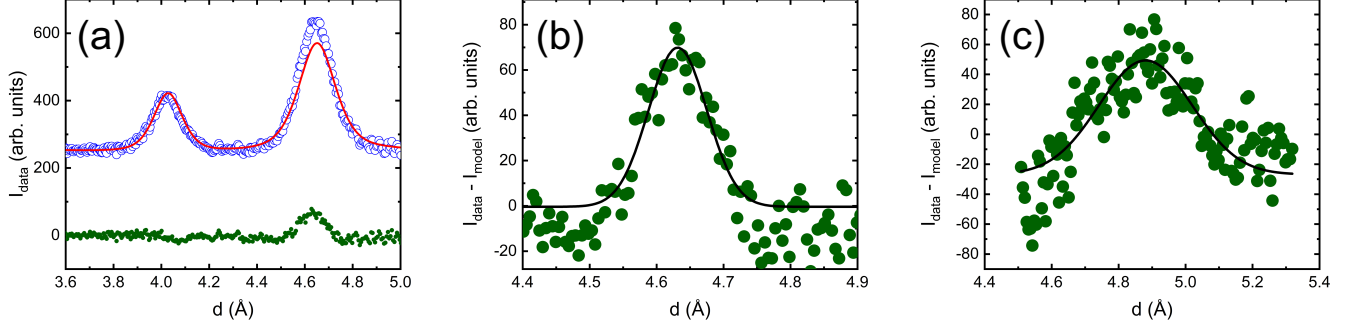


FIG. S3. (a) Expanded view of the neutron powder diffraction data collected at 10 K for the spherical nanoparticles, with experimental data as blue open circles, the calculated pattern in red, and the difference curve in green. (b) The fit of the difference curve from (a) using a Gaussian function centered at 4.7 Å. (c) The same as (b), but for the cubic nanoparticles at 10 K.

V. RESULTS OF PDF DATA REFINEMENTS

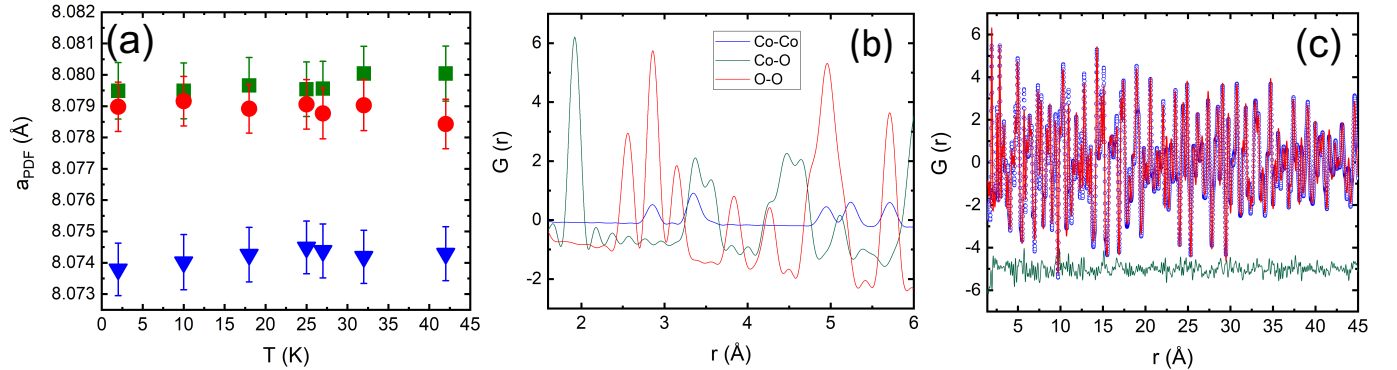


FIG. S4. (a) Temperature dependence of the lattice constant for all samples obtained from PDF data refinements. (b) Calculations of the partial PDFs for Co-O, Co-Co and O-O pairs based on the bulk structure of Co_4O_4 at 10 K. (c) Refined neutron PDF data at 10 K for the bulk powder.

VI. CNCS DATA

This data was collected at CNCS spectrometer at Spallation Neutron Source in Oak Ridge National Laboratory.

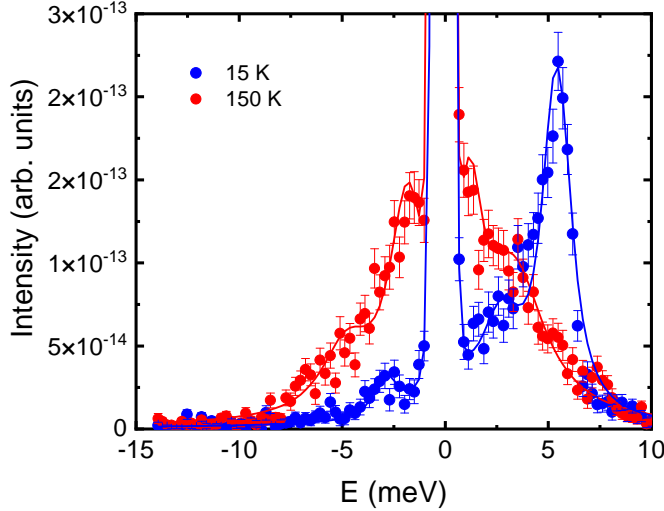


FIG. S5. CNCS data at 15 and 150 K for cubic nanoparticles. The solid lines are guides for the eye.

VII. MODELLING OF INELASTIC NEUTRON SCATTERING DATA

The bosonic Hamiltonian in the momentum space can be obtained as

$$H = -\frac{1}{2} \sum_q \psi_q^+ \mathcal{H}_q \psi_q$$

where,

$$\psi_q^+ = (a_{q1}^+ a_{q2}^+ a_{q3}^+ a_{q1}^+ b_{-q-1}^+ b_{-q-2}^+ b_{-q-3}^+ b_{-q-4}^+)$$

$$\mathcal{H} = S \begin{pmatrix} A & B & C & D & E & F & G & H_0 \\ B^* & A & D & C & F & E & H_0 & G \\ C^* & D^* & A & B & G & H_0 & E & F \\ D^* & C^* & B^* & A & H_0 & G & F & E \\ E^* & F^* & G^* & H_0^* & A & B & C & D \\ F^* & E^* & H_0^* & G^* & B^* & A & D & C \\ G^* & H_0^* & E^* & F^* & C^* & D^* & A & B \\ H_0^* & G^* & F^* & E^* & D^* & C^* & B^* & A \end{pmatrix}$$

with

$$\begin{aligned} A &= 4J_{AFM} - 12J_{FM} - 2D_S \\ B &= J_{AFM}(e^{i\pi q_y + i\pi q_z} + e^{-i\pi q_y + i\pi q_z} + e^{-i\pi q_y - i\pi q_z} + e^{i\pi q_y - i\pi q_z}) \\ C &= J_{FM}(e^{-i\pi q_x + i\pi q_z} + e^{i\pi q_x + i\pi q_z} + e^{i\pi q_x - i\pi q_z} + e^{-i\pi q_x - i\pi q_z}) \\ D &= J_{FM}(e^{-i\pi q_x + i\pi q_y} + e^{i\pi q_x - i\pi q_y} + e^{-i\pi q_x - i\pi q_y} + e^{-i\pi q_x + i\pi q_y}) \\ E &= J_{AFM}e^{-0.5i\pi q_x + 0.5i\pi q_y - 0.5i\pi q_z} \\ F &= J_{AFM}e^{-0.5i\pi q_x - 0.5i\pi q_y + 0.5i\pi q_z} \\ G &= J_{AFM}e^{0.5i\pi q_x + 0.5i\pi q_y + 0.5i\pi q_z} \\ H_0 &= J_{AFM}e^{0.5i\pi q_x - 0.5i\pi q_y - 0.5i\pi q_z} \end{aligned}$$

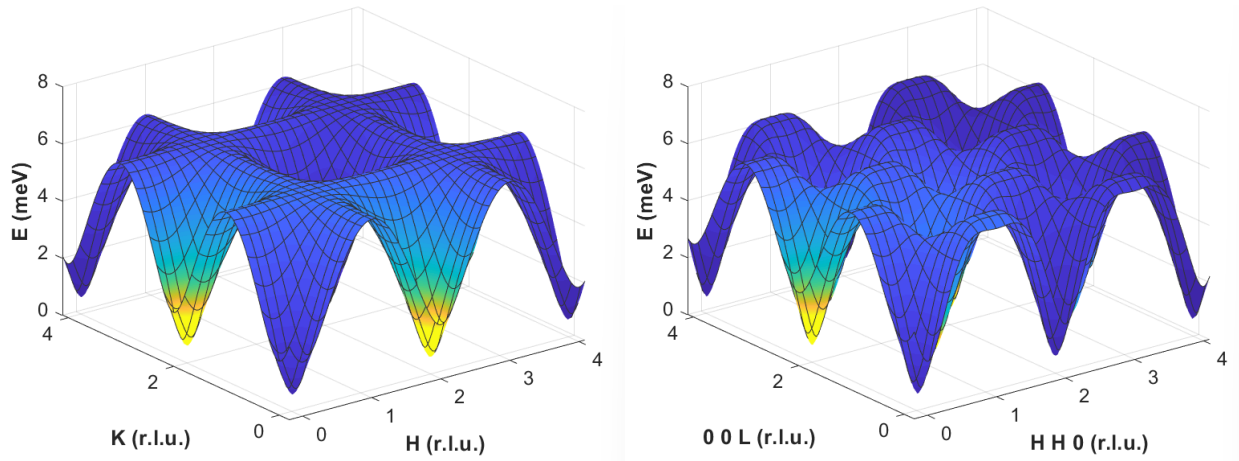


FIG. S6. Calculated spin-wave dispersion relation of Co_3O_4 over the Brillouin zone of its cubic lattice.

VIII. ADDITIONAL INS DATA AND SIMULATIONS

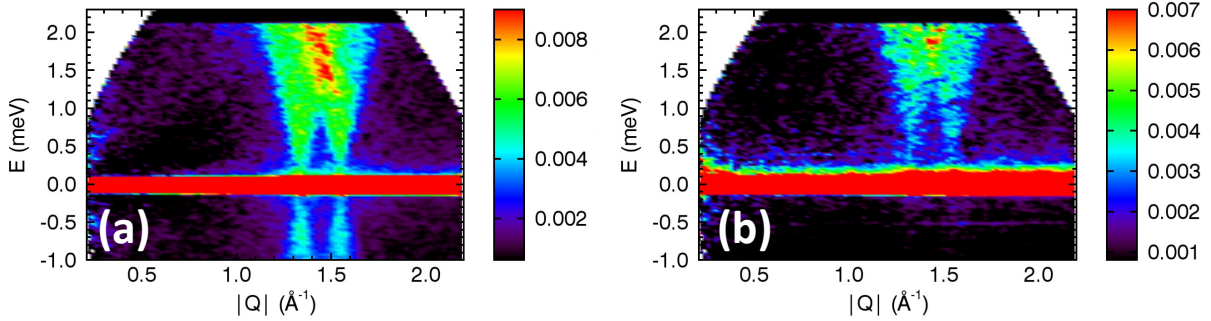


FIG. S7. The scattered intensity $I(Q, E)$ at 5 K for the (a) bulk powder at 25 K and (b) spherical nanoparticles at 5 K, measured with the high-resolution mode ($E_i = 3.4$ meV) at TOFTOF instrument.

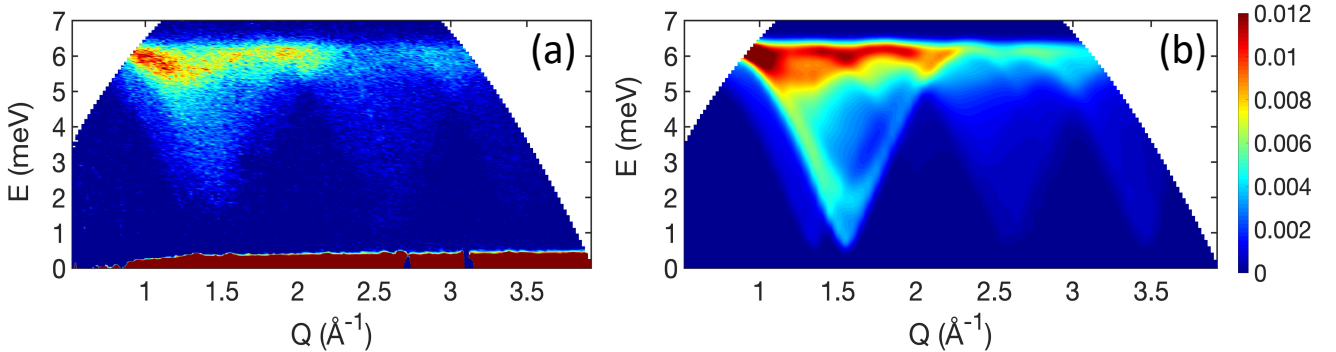


FIG. S8. The scattered (a) and calculated (b) intensity $I(Q, E)$ at 5 K for the cubic nanoparticles.

IX. BOXCAR REFINEMENTS OF PDF DATA

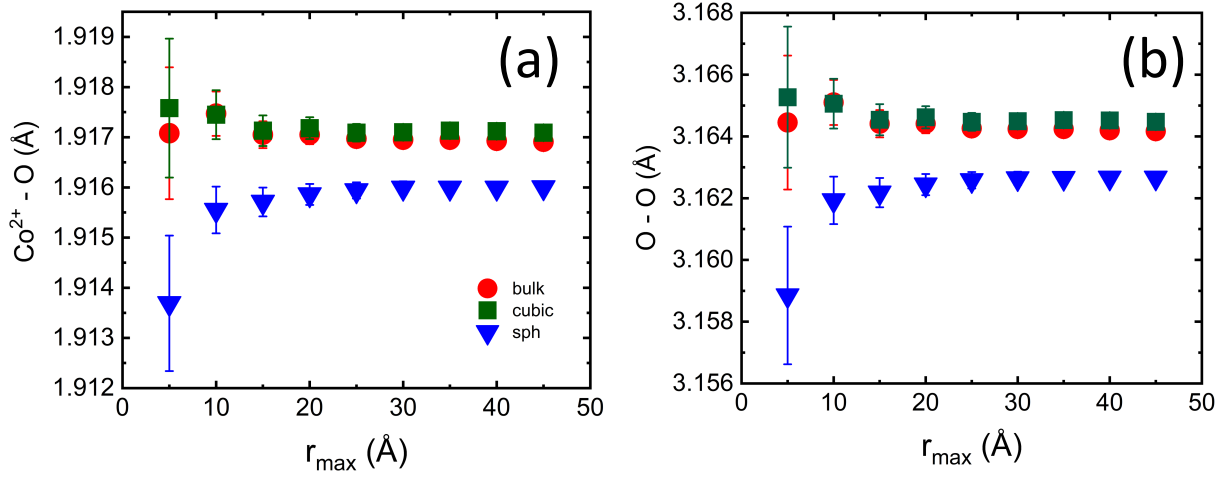


FIG. S9. (a) Co-O and (b) O-O bond lengths obtained from PDF data boxcar refinements at 10 K, as a function of r_{max} .

-
- [1] C. F. Windisch, G. J. Exarhos, R. R. Owings, *Journal of Applied Physics* **2004**, *95*, 10 5435.
- [2] S. R. Gawali, A. C. Gandhi, S. S. Gaikwad, J. Pant, T.-S. Chan, C.-L. Cheng, Y.-R. Ma, S. Y. Wu, *Scientific Reports* **2018**, *8*, 1 249.
- [3] C. Stella, N. Soundararajan, K. Ramachandran, *AIP Advances* **2015**, *5*, 8 087104.
- [4] C. F. Windisch, G. J. Exarhos, S. K. Sharma, *Journal of Applied Physics* **2002**, *92*, 9 5572.
- [5] B. Rivas-Murias, V. Salgueiriño, *Journal of Raman Spectroscopy* **2017**, *48*, 6 837.
- [6] M. A. Laguna-Bercero, M. L. Sanjuán, R. I. Merino, *Journal of Physics: Condensed Matter* **2007**, *19*, 18 186217.
- [7] Y. Zhao, M. Rashad, M. Rüsing, G. Berth, K. Lischka, A. Pawlis, *Journal of Nanomaterials* **2013**, *2013* 714853.
- [8] C. W. Na, H.-S. Woo, H.-J. Kim, U. Jeong, J.-H. Chung, J.-H. Lee, *CrystEngComm* **2012**, *14* 3737.